npg

Early otic development depends on autophagy for apoptotic cell clearance and neural differentiation

MR Aburto[1,2,3,6], H Sánchez-Calderón[1,2,6], JM Hurlé[4], I Varela-Nieto*[,1,2,5] and M Magariños[1,2,3]

Autophagy is a highly regulated program of self-degradation of the cytosolic constituents that has key roles during early development and in adult cell growth and homeostasis. To investigate the role of autophagy in otic neurogenesis, we studied the expression of autophagy genes in early stages of chicken (*Gallus gallus*) inner ear development and the consequences of inhibiting the autophagic pathway in organotypic cultures of explanted chicken otic vesicles (OVs). Here we show the expression of autophagy-related genes (Atg) *Beclin-1* (*Atg6*), *Atg5* and LC3B (*Atg8*) in the otocyst and the presence of autophagic vesicles by using transmission electron microscopy in the otic neurogenic zone. The inhibition of the transcription of LC3B by using antisense morpholinos and of class III phosphatidylinositol 3-kinase with 3-methyladenine causes an aberrant morphology of the OV with accumulation of apoptotic cells. Moreover, inhibition of autophagy provokes the misregulation of the cell cycle in the otic epithelium, impaired neurogenesis and poor axonal outgrowth. Finally, our results indicate that autophagy provides the energy required for the clearing of neuroepithelial dying cells and suggest that it is required for the migration of otic neuronal precursors. Taken together, our results show for the first time that autophagy is an active and essential process during early inner ear development.

Auditory and vestibular organs have a common developmental origin at the otic placode. The otic placode thickens, invaginates and forms the otic cup, which will close to form the otic vesicle (OV). Otic cells sequentially acquire the molecular characteristics that determine cell fate commitment resulting in the formation of hair cells and otic neurons.[1] Auditory and vestibular neurons will form two distinct ganglia of the peripheral nervous system to connect the highly specialized sensory epithelia with the central sensory pathways.[2] Neuroepithelial otic progenitors transit through states of cell proliferation, cell fate specification, cell cycle exit, migration and differentiation. Apoptosis contributes to the mechanics of morphogenesis, facilitates neuroblast migration and controls neuroepithelial cell numbers.[2–4] These developmental processes are orchestrated by factors that regulate intracellular signaling networks. Insulin-like growth factor I (IGF-I) modulates cell survival, epithelial morphogenesis, neurogenesis and late neural differentiation.[5–7] Mutations in the human and mouse genes coding for IGF-I cause syndromic sensorineural deafness.[8,9]

Autophagy is a catabolic process that supplies energy during development and in response to nutrient stress by carrying out lysosomal degradation of cell contents. Autophagy also has a housekeeping role preventing the accumulation of proteins and clearing damaged organelles and even cells.[10–12] Accordingly, autophagy in vertebrates has key roles in development,[13–15] cancer[16] and neuronal degeneration.[17] Autophagy begins with the formation of a phagophore that expands to form a double-membrane autophagosome. This engulfs intracellular cargo, such as protein aggregates, and organelles. The class III phosphatidylinositol 3-kinase participates in autophagosome formation by promoting the nucleation of autophagic vesicles. The autophagosome then fuses with a lysosome and acid hydrolases degrade its contents. Atg proteins participate at different stages of this process;[18] Beclin-1 (Atg6) associates with the phosphatidylinositol 3-kinase complex, leading to activation of microtubule-associated protein light chain 3 (LC3), a homolog of yeast Atg8, and membrane translocation. The cleavage of LC3 yields the cytosolic form, LC3-I that it is finally modified with phosphatidylethanolamine constituting the membrane-bound form LC3-II. This protein–lipid complex forms part of the double-membrane autophagosome, and thus the relative levels of LC3-II are a read-out of the number of

[1]Instituto de Investigaciones Biomédicas 'Alberto Sols', CSIC-UAM, Madrid, Spain; [2]CIBERER, Unit 761, Instituto de Salud Carlos III, Madrid, Spain; [3]Departamento de Biología, Universidad Autónoma de Madrid, Madrid, Spain; [4]Departamentos de Anatomía y Biología Celular, Universidad de Cantabria, Santander, Spain and [5]IdiPAZ, Madrid, Spain
*Corresponding author: I Varela-Nieto, Institute for Biomedical Research 'Alberto Sols', Consejo Superior de Investigaciones Científicas (CSIC), Universidad Autónoma de Madrid (UAM), Arturo Duperier 4, Madrid 28029, Spain. Tel: +34 915854421; Fax: +34 915854401; E-mail: ivarela@iib.uam.es
[6]These authors contributed equally to this work.

autophagosomes.[19] Mice with targeted mutations in *Atg5* and *Atg7* survive during embryonic development but die soon after birth, suggesting that both genes are important for survival during the early neonatal starvation period.[20,21] Embryos with mutations in *Beclin-1* die during early development,[22] and homozygous mutations in *Ambra1*, a ligand of Beclin-1, leads to severe neural tube defects and causes embryonic lethality.[23] The stages of autophagy can be characterized by these molecular markers and can be dissected by using both genetic tools and chemical inhibitors. Among the latest are 3-methyladenine (3-MA), which blocks early stages in the autophagic process, and chloroquine (CQ), which prevents the fusion of autophagosomes with lysosomes, resulting in an accumulation of autophagosomes and inhibition of autophagy.[24] In the inner ear, information on the possible roles and mechanisms of regulation of autophagy is limited. Autophagin-1/Atg4B-deficient mice show balance alterations.[25] Gene expression studies in the E18.5 cochlea have shown the expression of key autophagy genes such as *Beclin*-1, *LC3B, FKBP11* and *Atg* genes, including *Atg4b* and *d*[6] (Gene Expression Omnibus accession number GSE11821). Autophagic cell death has also been reported in the organ of Corti after treatment with ototoxic compounds,[26] indicating important roles for this process in development and homeostasis of the inner ear.

Here we show that *Atg5*, *Beclin-1* and LC3B are expressed during early development of the chicken inner ear. The otic epithelium shows intense lysosomal activity and numerous autophagic vesicles, especially at the neuroblasts exit zone. Accordingly, autophagy inhibition in *ex ovo* cultures by using both genetic and pharmacological approaches causes the accumulation of apoptotic cells. OV developmental processes could not progress when autophagy was inhibited, and the explants showed aberrant morphologies both at the epithelial neurogenic zone and within the embryonic acoustic-vestibular ganglia (AVG). Addition of methyl pyruvate (MP) abrogated the consequences of autophagy inhibition. These results show for the first time that autophagy is an active process during early inner ear development that provides the energy required for the clearing of dead neuroepithelial cells and for the generation of neuronal otic precursors.

Results

Autophagy machinery is expressed during early otic development. Figure 1 shows the expression of key autophagy genes during the formation of the OV and early otic neurogenesis stages (Figure 1A a). *Atg5* and *Beclin-1* expression was shown by quantitative RT-PCR and when indicated by immunohistochemistry in chicken embryos (Figures 1A b and c). Beclin-1 showed a cytosolic punctuate staining in the otic epithelium and in the dorsal region of AVG of HH18 embryos (Figure 1A b). Incubation of just-isolated HH18 otocyst shows the presence of LC3B labeling (Figure 1A d). Transmission electron microscopy of the neurogenic zone showed a loose package of the epithelial cells with a set of pale cytolytic cells, which presented a heavily vacuolized cytoplasm (Figure 1A e′, asterisk). Round cells detaching from the epithelium were also observed (Figure 1A e′, arrow). Epithelial cells presented both

autophagosomes in formation (omegasomes, Figure 1A e″) and double-membrane accumulation of vacuoles with remaining cytoplasmic contents (Figure 1A e‴, arrow).

MDC is an autofluorescent amine that stains autophagosomes.[27] Cultured OVs proceed with neurogenesis and develop the AVG (schematic representation in Figure 1B a), both the neurogenic and proximal regions of the otocyst were labeled with MDC (Figure 1B b, upper panels). Exposure to 3-MA strongly reduced MDC staining and LC3B levels (Figure 1B b, upper and lower panels, respectively). To discard non-specific effects of 3-MA, the findings were confirmed by silencing LC3B using Morpholino antisense oligonucleotides (Supplementary Figure S1). Panel A shows the uptake of the control FITC-conjugated MO, whereas panel B shows the reduction of MDC and LC3B in LC3-MO-exposed OVs (compare a and b with d and e, respectively). LC3-II is expressed in 0S OV cultures and the addition of CQ during the last 4 h of culture further increased the levels of LC3-II, indicating that there is autophaghic flux under these conditions. Treatment with 3-MA blocked the conversion of LC3-I to LC3-II (Figure 1B c).

Inhibition of autophagy increases TUNEL labeling in the OV. Next, we studied whether autophagy has a role in cell survival during early inner ear development. TUNEL labeling was performed on cultured OVs in the 0S condition or in the presence of IGF-I, 3-MA or a combination of both (Figure 2A). OVs exposed to 3-MA showed an increased TUNEL staining (Figure 2A, compare c′ and a′), with abundant cell death in the AVG and in the otic epithelium (Figure 2A c′). AVG from the 3-MA-exposed OVs showed an abnormal morphology, with accumulations of cells adhered to the otic epithelium (Figures 2A c and d). The number of apoptotic TUNEL-positive cells found in the 3-MA vesicles was 3.6-fold higher than that found in the 0S condition (Figure 2A, quantification in e). The inhibition of autophagy with an LC3B antisense MO also increased significantly the number of TUNEL-positive cells (Supplementary Figure S1 B c, f and quantification in g).The addition of IGF-I promoted cell survival and caused an increase in OV size (Figures 2A a–a′ and b–b′). IGF-I decreased 1.4-fold the apoptosis induced by 3-MA (Figures 2A d′ and c′ and quantification in e), and the aberrant cell accumulations were also reduced (Figure 2A c and d). IGF-I also reduced the amount of MDC staining when compared with the control condition (data not shown).

Cell death was significantly reduced by the pan-caspase inhibitor BOC by 12.5-fold in the 0S condition and by 12.7-fold in the 3-MA condition (Figures 2B a–d, quantification in e). Apoptosis was further studied by combining TUNEL staining with the immunodetection of active caspase-3. The 3-MA-treated OVs showed areas of apoptotic cell death where TUNEL-labeled apoptotic nuclei were surrounded by cytoplasm containing active caspase-3 (Figure 2B f).

Apoptotic otic cells accumulate in the OV upon 3-MA treatment. The exposure of phosphatidylserine (PS) on the surface of apoptotic cells triggers engulfment by phagocytes and can be labeled with annexin-V.[28] Cultured OVs showed annexin-V staining associated with areas of TUNEL-positive
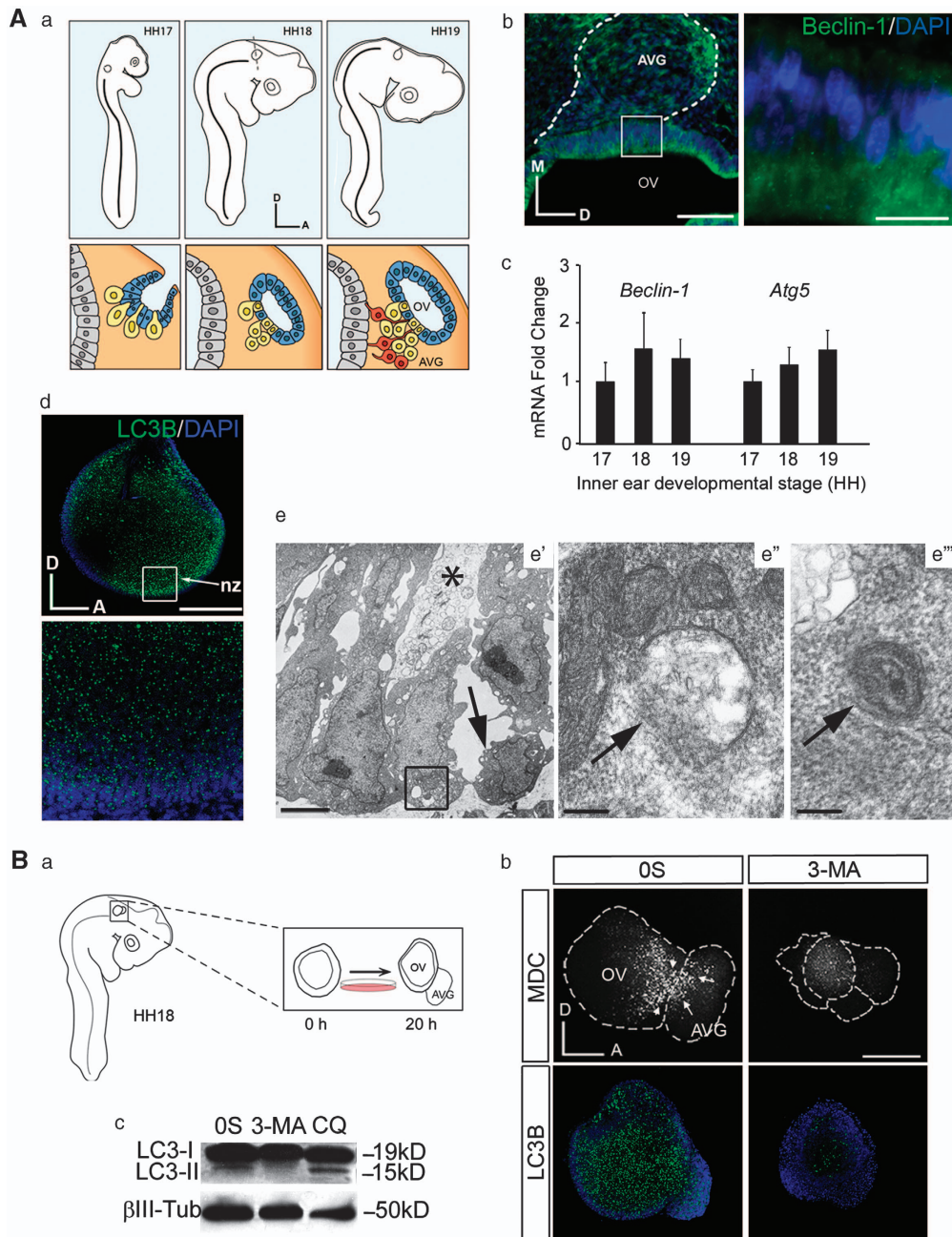
Figure 1 Autophagy during early inner ear development. **(A)** (a) Schematic drawings showing the development of the chicken inner ear at the Hamburger and Hamilton stages HH17–HH19. The lower panels represent otic vesicle development at these HH stages and neuroblast delamination from the ventromedial aspect of the otic epithelium to form the AVG. (b) Immunofluorescence of Beclin-1 in cryostat serial sections at HH18 showing its location at the otic epithelium and within the AVG. Boxed area shows Beclin-1 punctuate staining in the luminal part of the otic epithelium. Bars = 75 and 20 μm, respectively. (c) *Beclin-1* and *Atg5* mRNA levels in the developing inner ear were measured by qRT-PCR at different stages. Gene expression was calculated as $2^{-\Delta\Delta Ct}$ and normalized to the levels at HH17. (d) Immunofluorescence of LC3B in the otic vesicle. LC3B is expressed in the otic epithelium, including the neurogenic zone (nz), which is also shown at a higher magnification. (e) Transmission electron microscopy of the neurogenic zone of the otic vesicle at stage HH18. (e′) Low magnification view showing the loose package of the epithelial cells at this region, resulting in the formation of large intercellular spaces. Note a pale degenerating cell (asterisk) and a cell in the process of detachment from the epithelium, probably a delaminating neuroblast (arrow). (e″) An omegasome (arrow), a double-membrane protrusion from cytoplasmic organelles that serves as a platform for autophagosome biogenesis. (e‴) An autophagic vesicle containing cytoplasmic remnants in the basal aspect of the otic epithelial cells. Bars = 3 μm (e′) and 0.2 μm (e″–e‴). **(B)** (a) Schematic representation showing the *ex vivo* culture of an explanted otic vesicle from an HH18 embryo. The AVG develops from the otic vesicle after 20 h in culture in serum-free culture medium (0S). (b) MDC and LC3B staining in autophagy-inhibited cultured otic vesicles. Otic vesicles were incubated for 20 h in the 0S condition or with 3-MA (10 mM). Arrowheads and arrows show MDC staining in the neurogenic region and in the AVG, respectively. 3-MA-exposed otic vesicles show highly reduced levels of MDC-labeled cells (upper panels) and of LC3B inmunostaining (green, lower panels). (c) Otic vesicles were isolated from HH18 embryos, made quiescent and cultured 20 h in the 0S condition or treated for 20 h with 3-MA (10 mM) or 4 h with CQ (10 μM). Cultured otic vesicle lysates were analyzed by western blotting to determine the levels of LC3-I and LC3-II; β-Tubulin (β-Tub) was used as a loading control. A representative blot of three independent experiments is shown. Orientation: A, anterior; D, dorsal; M, medial. Bar = 150 μm
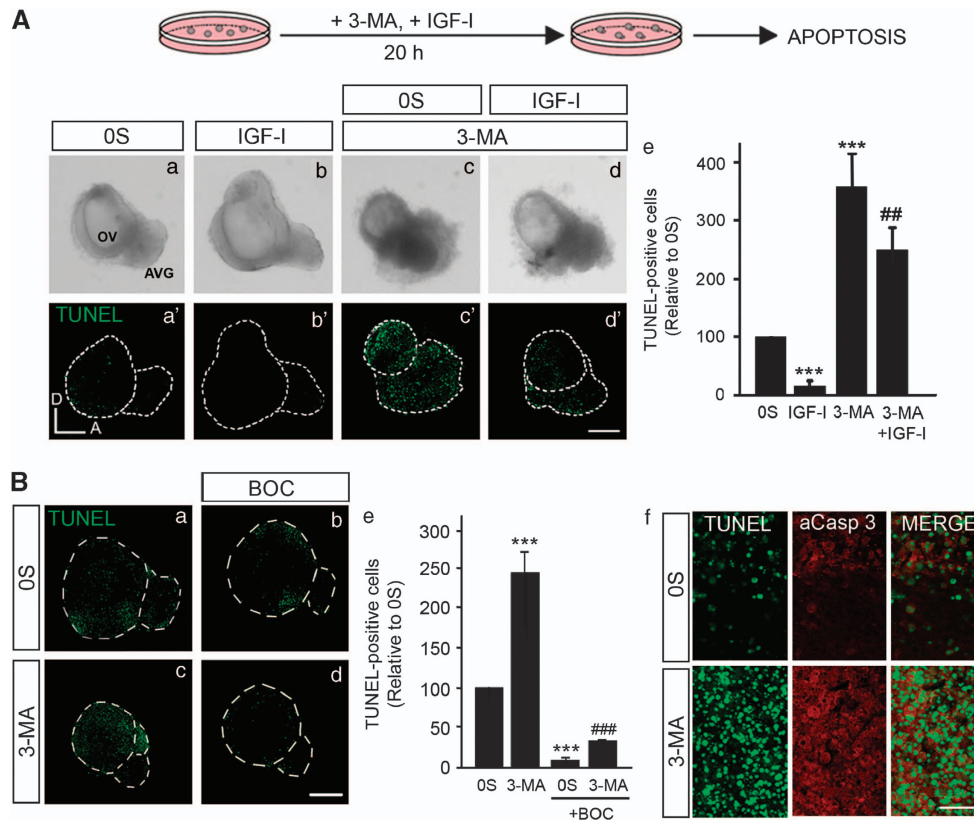
Figure 2 Inhibition of autophagy increases TUNEL-positive cells in cultured otic vesicles. (**A**) The schematic drawing shows the experimental design. (a–d, a'–d') Otic vesicles were isolated from HH18 chicken embryos, made quiescent and cultured for 20 h in the 0S condition with IGF-I (10 nM), 3-MA (10 mM) or a combination of both. Apoptotic cell death was visualized by TUNEL (green). Bar = 150 μm. (e) TUNEL-positive nuclei were quantified with Image Analysis Software (Olympus, Tokyo, Japan) relative to the 0S condition, which was given an arbitrary value of 100. Data are the mean ± S.E.M. of at least five otic vesicles from the conditions shown. Statistical significance was estimated with the Student's *t*-test: ***P < 0.005 versus 0S, ##P < 0.01 versus 3-MA 10 mM. (**B**) (a–d) Otic vesicles were isolated from HH18 chicken embryos and cultured for 20 h in the 0S condition in the presence of 3-MA (10 mM) alone or in combination with the pan-caspase inhibitor BOC (50 μM). Cell death was visualized using the TUNEL technique. Bar = 150 μm. (e) TUNEL-positive nuclei were quantified with Image Analysis Software (Olympus, Tokyo, Japan) relative to the 0S condition, which was given an arbitrary value of 100. Data are the mean ± S.E.M. of at least three otic vesicles from the conditions shown. Statistical significance was estimated with the Student's *t*-test: ***P < 0.005 versus 0S, ###P < 0.005 versus 3-MA 10 mM. (f) Apoptotic cell death visualized by TUNEL staining (green) and immunostaining for activated-caspase-3 (red) of a selected region from the otic vesicles cultured in 0S or in the presence of 3-MA 10 mM. Bar = 20 μm. Compiled projections of confocal microscopy images from otic vesicles are shown. Orientation: A, anterior; D, dorsal. The images shown are representative of at least three independent experiments, using 5–6 otic vesicles per condition

cells (Figures 3A a–c, a'–c'). By contrast, treatment with 3-MA increased TUNEL labeling accompanied by a significant reduction of annexin-V in the otocyst (Figures 3A d–f, d'–f', quantification in g). 0S OVs showed lysosomal LTR-labeling associated to TUNEL staining (Figures 3B a–c, a'–c') that was significantly reduced in 3-MA-treated OVs (Figures 3B d–f, d'–f', quantification in g).

These results indicate that inhibition of autophagy impedes PS-exposure in the surface of dying cells, which precludes the engulfment of apoptotic cells by phagocytes, resulting, therefore, in an accumulation of TUNEL-positive cells.

Inhibition of autophagy causes cell cycle misregulation in the OV. To study the effects of autophagy on cell cycle, OVs were cultured in the presence of BrdU or labeled for the mitotic marker phospho-histone 3. In cultured OVs, IGF-I mediates proliferation of ganglionar neuroblasts by the

activation of the RAF/MAPK pathway.[29] 3-MA-treated OVs showed a significant reduction of cells expressing phospho-histone 3 (Figure 4A, compare c with a; quantification in e). Different exposure times to BrdU (45 min, 3 and 6 h) showed that 3-MA induced proliferation at all the times tested (Figure 4B). Furthermore, 3-MA treatment showed an accumulation of BrdU in the neuroblast delamination zone (Figure 4B, arrows).

Autophagy is required for otic neurogenesis. To explore the role of autophagy on neurogenesis, we studied the expression of neural markers characteristic of the sequential transit from epithelial neuroblasts to mature neurons that follow a spatiotemporal gradient (Figure 5). SOX2 maintains self-renewal of undifferentiated cells and is expressed in the otic proneural domain.[30] Islet-1 is expressed by epithelial and ganglionar neuroblasts,[31] whereas the β-III-tubulin, TuJ-1, and the neurofilament G4 are expressed by the neurons and
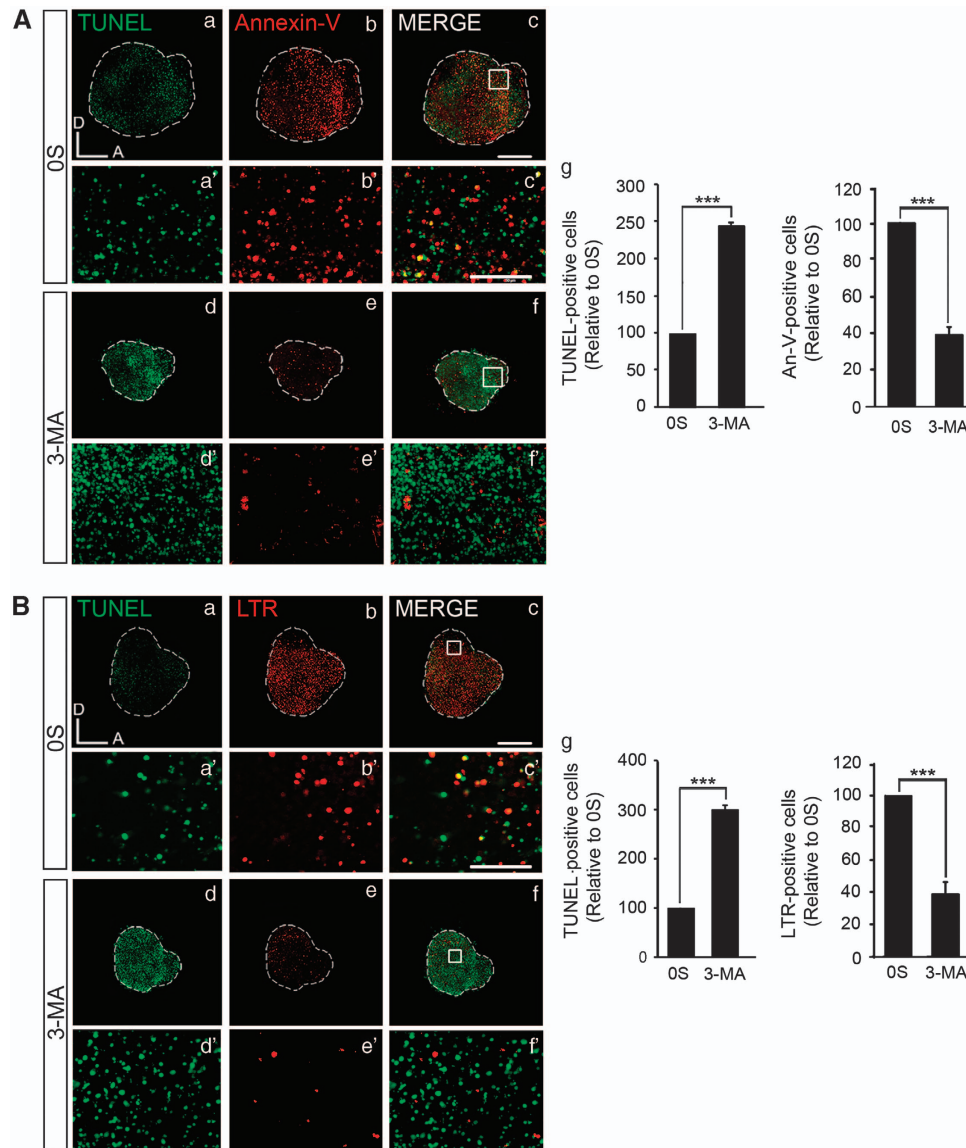
Figure 3 Inhibition of autophagy prevents annexin-V exposure and subsequent phagocytosis of apoptotic cells. (**A**) (a–f) Otic vesicles were explanted from stage HH18 chicken embryos and incubated for 20 h in the 0S condition or with 3-MA 10 mM. The explants were then incubated with annexin-V (red) the last 30 min in culture. Apoptotic cell death was visualized by TUNEL (green) in cultured otic vesicles (a′–f′) Higher magnification of the selected regions shown in the boxed areas in c and f, respectively. (g) Histograms show the quantification of TUNEL- and annexin-V-positive cells relative to the 0S condition, which was given an arbitrary value of 100. Data are the mean ± S.E.M. of at least five otic vesicles from the conditions shown. Statistical significance was estimated with the Student's t-test: ***$P < 0.005$ versus 0S. (**B**) (a–f) Cultured otic vesicles without additions (0S) or in the presence of 3-MA (10 mM) were incubated with 1 μM LTR for the last 15 min of culture. Apoptotic cell death was visualized by TUNEL (green). (a′–f′) Higher magnification of the selected regions shown in the boxed areas in c and f, respectively. (g) The TUNEL- and LTR-positive cells were quantified and data are shown relative to the 0S condition, which was given an arbitrary value of 100. Data are shown as the mean ± S.E.M. of at least five otic vesicles. Statistical significance was estimated with the Student's t-test: ***$P < 0.005$ versus 0S. Compiled projections of confocal microscopy images from otic vesicles are shown. The images shown are representative of at least two independent experiments, using 5–6 otic vesicles per condition. Orientation: A, anterior; D, dorsal. Bar = 150 μm

the pioneer axons that innervate the sensory patches at the otic epithelium[32] (Figure 5A c arrows).

The inhibition of autophagy with 3-MA altered the pattern of expression of Islet-1, TuJ-1, SOX2 and G4 in the otocyst (Figures 5A and B). The AVG showed a reduced size and accumulations of cells adhered to the otic epithelium. These cells were negative for the neural markers Islet-1 and TuJ-1 and show fragmented nuclei (Figures 5A f–h, inset in g).

Furthermore, the axons from the 3-MA-treated AVG showed an abnormal pattern of axonal guidance, projecting to the aberrant accumulations of cells instead of innervating the otic epithelium (Figure 5A h arrows). Accordingly, treatment of AVG explants with 3-MA caused a dramatic reduction in the growth of neuronal processes (Figure 5C).

To determine whether the abnormal ganglia phenotype triggered by 3-MA was reversible, the inhibitor was removed
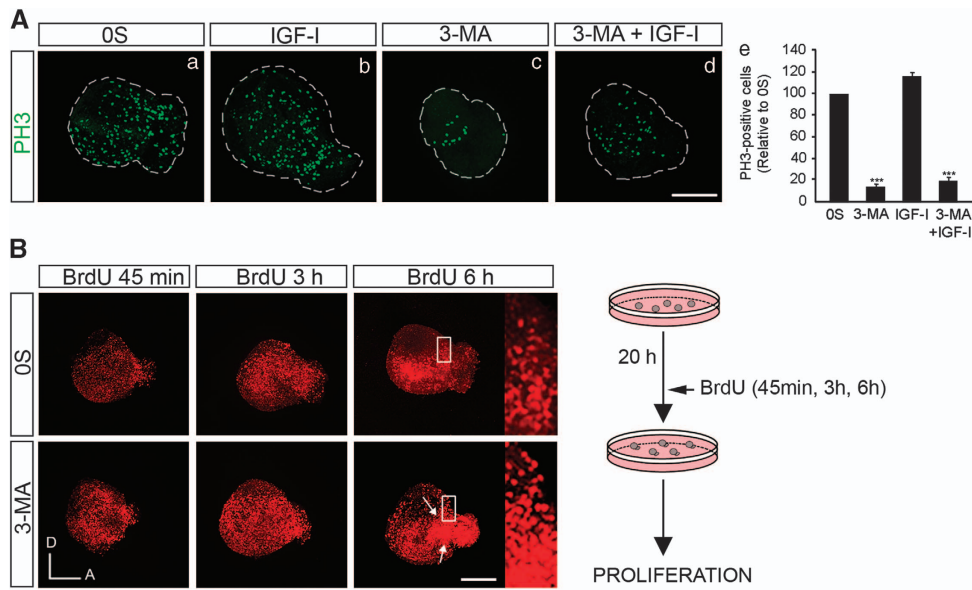
Figure 4 Inhibition of autophagy causes cell cycle misregulation. (**A**) (a–d) Otic vesicles were isolated from HH18 chicken embryos and incubated for 20 h in the 0S condition with IGF-I (10 nM), 3-MA (10 mM) or a combination of both. Proliferation was followed by the mitosis marker phospho-histone 3 (PH3; green). (e) PH3-labeled cells were quantified with Image Analysis Software (Olympus, Tokyo, Japan) in at least five otic vesicles per condition. The results are shown as the mean ± S.E.M. relative to the 0S condition, which was given an arbitrary value of 100. Statistical significance was estimated with the Student's *t*-test: ***$P < 0.005$ versus 0S. (**B**) Otic vesicles cultured in the 0S and 3-MA conditions were assayed for BrdU immunoreactivity after 45 min, 3 and 6 h of exposure to BrdU. Arrows show BrdU staining in the neurogenic region and in the AVG. Compiled projections of confocal microscopy images from otic vesicles are shown. Boxed area indicates the region of the otic vesicle selected to show the BrdU-positive nuclei. The schematic drawing shows the experimental design. The images shown are representative of at least two independent experiments, using 5–6 otic vesicles per condition. Orientation: A, anterior; D, dorsal. Bars = 150 μm

and fetal bovine serum was added (schematic representation of culture procedure in Figure 5A k). AVG showed a partial recovery but were still smaller than control AVG (Figure 5A, quantification in l), which presented a differentiated state showing two intense TuJ-1 regions, which presumably are vestibular and acoustic regions (Figure 5A e, arrowheads). After addition of fetal bovine serum, the aberrant accumulations of cells adhered to the otic epithelium disappeared (Figures 5A i–j).

Restoration of ATP levels by MP reverses autophagy inhibition. To analyze the contribution of autophagy to metabolic energy supplies during otic development, the effects of MP as an ATP source upon 3-MA treatment were evaluated as reported previously by others.[10,33]

Programmed cell death, phagocytosis of apoptotic cells, proliferation and neurogenesis were analyzed. The presence of MP significantly reduced cell death in the 0S condition (1.7-fold; Figures 6A a and g, quantification in m) and partially rescued the explants from the effects of 3-MA as the number of TUNEL-positive cells was significantly reduced by 3.4-fold (Figures 6A d, j, quantification in m). LTR-labeling was significantly reduced in 3-MA-treated OVs by threefold (Figures 6A b, e, quantification in n), whereas it was significantly increased by twofold upon MP addition (Figures 6A e, k, quantification in n).

Neurogenesis, evaluated by the expression of Islet-1 and TuJ-1, was improved in the presence of MP (Figures 6B a–c, quantification in d). These results indicate that supplying an energy source rescues the disruption to the developmental program caused by the inhibition of autophagy.

Discussion

Autophagy mediates bulk protein and organelle turnover, helping cells in the cytosolic remodeling that is crucial to cell fate specification and differentiation. We show here for the first time that autophagy provides energy for the clearing of dying cells and enables neuronal differentiation during early otic development.

Beclin-1 and *Atg5* transcripts are expressed during early inner ear development and at HH18. Accordingly, Beclin-1 and LC3B are expressed in the otic epithelium and in the AVG, where intense lysosomal activity was particularly observed at the neurogenic zone. Transmission electron microscopic study of this area confirmed the presence of omegasomes, autophagic vacuoles and dying cells, showing a clear cytoplasm that might be opening spaces at the neurogenic zone for epithelial neuroblasts to exit the epithelium and migrate. These data suggest that autophagy is having a key role in shaping the otic epithelium and facilitating the process of neurogenesis. Organotypic cultures of OVs maintained in a deprived medium showed autophagosomes at the neurogenic region and the activation of LC3-I to LC3-II. Furthermore, 3-MA inhibition of autophagy prevented the formation of late autophagic vacuoles and LC3-II conversion, whereas exposure to CQ induced LC3-II accumulation. In addition, knockdown of LC3B expression by using antisense morpholinos
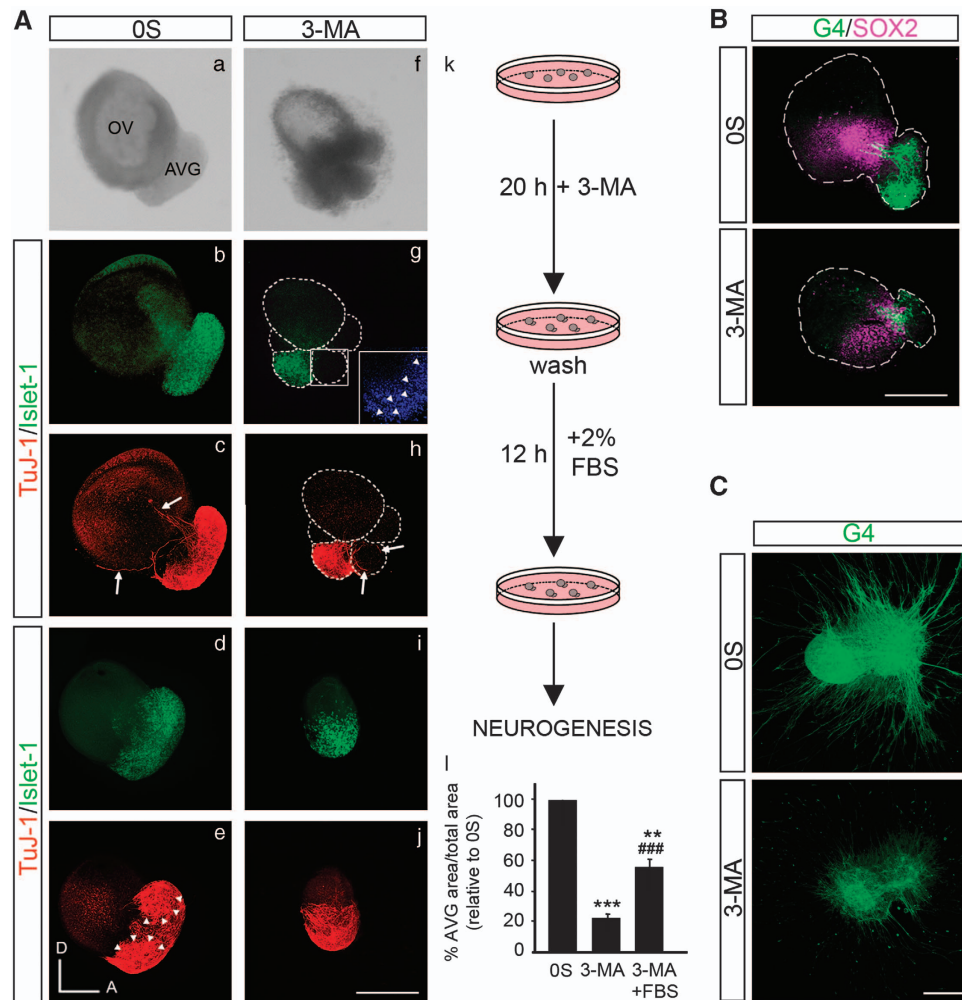
Figure 5 Autophagy inhibition impairs AVG formation. (**A**) (a–j) Otic vesicles were isolated from HH18 chicken embryos and incubated in the 0S condition or with 3-MA (10 mM) for 20 h. Secondly, they were washed briefly and were again incubated for 12 h in fresh medium with 2% of fetal bovine serum (FBS). Whole otic vesicles were then immunostained for the ganglion neuroblast nuclei marker Islet-1 (green) and for the marker of neural processes, TuJ-1 (red). The boxed area (g) shows a higher magnification of a region adjacent to the neural area where fragmented nuclei (visualized by DAPI, arrowheads) can be observed. Arrows show the neural processes extending towards the otic epithelium (c) and towards the accumulation of dead cells (h). Arrowheads in (e) highlight the AVG vestibular and acoustic regions. (k) The schematic drawing shows the experimental design. (l) AVG and OV areas were quantified (as described in the Materials and Methods section) and referred to the total area to compare the AVG size under the different culture conditions. The results were normalized to the 0S condition, which was given an arbitrary value of 100. The bars show the mean ± S.E.M. of at least five otic vesicles from any of the conditions shown. Statistical significance was estimated with the Student's t-test: **$P < 0.01$, and ***$P < 0.005$ versus 0S and ###$P < 0.005$ versus 3-MA. Bar = 150 μm. (**B**) Double immunostaining of otic vesicles cultured under the above conditions was carried out for the transcription factor SOX2 (magenta), expressed in the proneural domain by otic precursors, and for the G4-glycoprotein used as a marker of neuronal processes (G4, green). Orientation: A, anterior; D, dorsal. Bar = 150 μm. (**C**) AVG explants were obtained from stage HH19^{+} chicken embryos and cultured in the 0S condition or with 3-MA (10 mM) for 20 h. Whole AVG explants were immunostained for G4 (green) to observe the sensory otic neuron processes. Bar = 300 μm. Fluorescence images were obtained from the compiled projections of confocal images of otic vesicles and acoustic-vestibular ganglia. Representative images of at least 5–6 samples per condition and from at least three independent experiments are shown

also shows a decrease of the autophagic read-outs LC3B and MDC, confirming that the autophagic machinery is present and active during inner ear development.

Autophagy is required for the clearance of apoptotic cells during inner ear development. Autophagy is a mechanism for adaptation to stress that prevents cell death,[34] but it may also trigger type II cell death.[35] Apoptosis has been shown to have an important role during early development of the inner ear; it contributes to the regulation of otic cell numbers and serves to remove aberrant cells;[2] however, studies addressing the role of autophagy in the

inner ear are limited. RNA microarray analysis in prenatal mouse cochlea showed the expression in E18.5 embryos of *Beclin-1*, *Atg3*, *Atg4b*, *Atg4d*, *Atg5*, *Atg7*, *Atg10*, *Atg12* and *Agt16* genes, as well as of the mechanistic target of rapamycin mTOR modulator FKBP11[6] (Gene Expression Omnibus accession number GSE11821). Dead cells with autophagic features have been observed in the damaged cochlea,[26] and autophagy genes are essential for vestibular function in mice.[25]

The inhibition of autophagy by LC3B genetic inhibition and by 3-MA increased the amount of apoptosis detected in the otocysts, whereas co-treatment with the caspase inhibitor
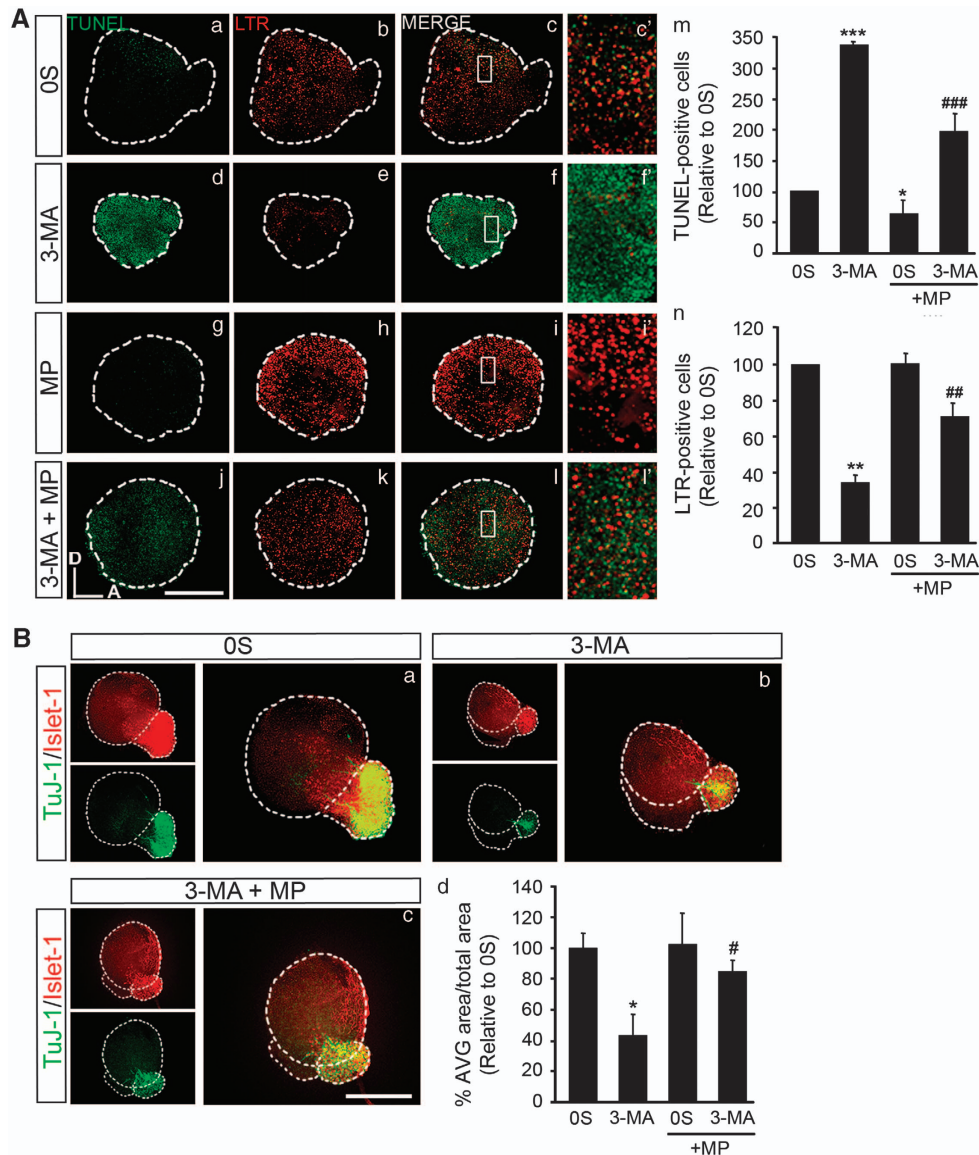
Figure 6 MP partially restores basal levels of TUNEL + cells and neurogenesis. (**A**) (a–l) Otic vesicles were isolated from HH18 chicken embryos and incubated for 17 h in the 0S condition. Then, they were cultured for 3 h in the presence or absence of 3-MA (10 mM), MP (10 mM) or a combination of both. Otic vesicles were incubated with 1 μM LTR (red) for the last 15 min of culture and apoptotic cell death was visualized by TUNEL (green). (c′, f′, i′ and l′) Higher magnification of the selected regions shown in the boxed areas of c, f, i and l, respectively. (m) TUNEL-positive cells and (n) LTR-positive cells were quantified with Image Analysis Software (Olympus, Tokyo, Japan) in at least five otic vesicles per condition. The results are shown as the mean $\pm$ S.E.M. relative to the 0S condition. Statistical significance was estimated with the Student's t-test: *$P < 0.05$, **$P < 0.01$ and ***$P < 0.005$ versus 0S and ##$P < 0.01$, ###$P < 0.005$ versus 3-MA. (**B**) (a–c) HH18 otic vesicles were incubated for 20 h in the 0S condition, with 3-MA (10 mM), MP (10 mM), or a combination of both. Whole otic vesicles were then immunostained for Islet-1 (green) and TuJ-1 (red) to label neuroblast nuclei and the neural processes, respectively. (d) AVG and OV areas were quantified (as described in the Materials and Methods section) and referred to the total area to compare the AVG size under the different culture conditions. The results were normalized to the 0S condition, which was given an arbitrary value of 100. The bars show the mean $\pm$ S.E.M. of at least five otic vesicles from any of the conditions shown. Statistical significance was estimated with the Student's t-test: **$P < 0.01$, and ***$P < 0.005$ versus 0S and ###$P < 0.005$ versus 3-MA. Compiled projections of confocal microscopy images from otic vesicles are shown. The images shown are representative of at least three independent experiments. Orientation: A, anterior; D, dorsal. Bars = 150 μm

BOC blocked cell death even in the presence of 3-MA and reduced the apparent loss of viability induced by autophagy suppression. The reduction of annexin-V and LTR staining in 3-MA-treated OVs indicated that deficient autophagy prevents PS exposure in the otocyst dying cells. Therefore, the engulfment of apoptotic cells by non-professional macrophages[36] does not occur and the dead-TUNEL-positive cells remained visible and accumulate attached to the epithelium.

Additionally, an increase in cell death caused by deficient autophagy may also contribute to the accumulation of apoptotic cells. Therefore, autophagy is required for apoptotic cell clearance possibly providing the required energy to expose PS at the cell surface. Indeed, autophagy generates amino acids needed for ATP production during nutrient starvation.[37] This hypothesis was confirmed by a set of experiments where external sources of nutrients or ATP were

tested and shown to rescue the aberrant phenotype caused by autophagy suppression in the OV. The number of dead cells was reduced, LTR staining was increased and the AVG was formed. The actions of 3-MA are reversible as fetal bovine serum could restore the phagocytosis of dead cells in the otic epithelium. These results indicate that autophagy has a key role in apoptotic corpse clearance during inner ear development, as described in other systems.[10,11]

Autophagy suppression causes cell cycle misregulation and impaired neurogenesis. OVs exposed to 3-MA showed a reduced size and a striking decrease in phospho-histone 3, a read-out of the G_2/M phase, whereas BrdU incorporation showed a time-dependent increase. These data indicate that otic precursors are able to pass the $G_1/$S-phase checkpoint but are unable to complete cell division, which will probably lead to increased apoptotic cell death. There are several mechanisms that could be underlying the consequences of autophagy inhibition on cell cycle. Defects in autophagy could deregulate the dynamics of microtubules, which are essential to complete the cell cycle.[37] Autophagy is also essential for cytosolic rearrangements, and in the absence of autophagy, otic progenitors may be unable to carry out differentiation and would initiate another proliferation round instead. Accordingly, the areas of the otocyst that show more intense BrdU staining are the neurogenic region and the AVG. The misregulation of the cell cycle secondary to defects in autophagy has been reported in the *Ambra1* mutants.[23] In the OV, the combination of increased cell proliferation without mitosis, accumulation of dead cell bodies and impaired neurogenesis cause the remarkable phenotype in the OV, including the accumulation of dead cells.

Exposure to 3-MA caused a dramatic alteration in the spatiotemporal pattern of expression of neural markers and a decrease in the size of the AVG, indicating that autophagy is essential for otic neurogenesis. In addition to the reduced population of neural precursors, our data suggest that blocking autophagy may also affect neuronal differentiation. The role of autophagy in promoting differentiation has been reported in *Ambra1* mutants,[23] as well as in mouse neuroblastoma cells.[38] Furthermore, the homolog for Atg1 in *Caenorhabditis elegans*, Unc-51, is required for axonal guidance.[39] Interestingly, suppression of autophagy impaired axonal outgrowth and altered the pattern of neuritogenesis and pathfinding in the cultured OV. In 0S-OVs, the neurons guide their axons towards the otic epithelium to innervate the different sensory patches of the inner ear, whereas the axons from 3-MA-treated OVs innervate other regions such as the accumulation of dead cells. Alternatively, these defects could be due to impaired neuronal homeostasis, which may depend on basal levels of autophagy, as described previously.[35,40]

IGF-I and autophagy in the OV. IGF-I promotes neural progenitors survival and expansion during otic development.[2] IGF-I reduced TUNEL-positive cells in 3-MA-exposed OVs but it was unable to recover other traits of autophagy. Thus, the levels of annexin-V staining were low, indicating that autophagy inhibition precludes PS-exposure even in the presence of IGF-I. Our data indicate that in the developing inner ear, growth factors may repress the autophagy

machinery because IGF-I reduced the amount of autophagosomes when compared with control conditions. Reducing apoptosis could make autophagic energy to expose PS dispensable and, therefore, the autophagic machinery is repressed. Comparative expression profiles of the mouse cochlea of E18.5 *Igf1* null and wild-type mice suggest that *Igf1* deficit slightly represses the expression of autophagy genes.[6] Further research would be needed to explore the regulation of autophagy by IGF-I during inner ear development.

In conclusion, to our knowledge, this is the first time that autophagy has been implicated in early otic inner ear morphogenesis where the demanding process of neurogenesis seems to be supported by the energy supplied by this process. Autophagy may be acting at complementary levels to support inner ear development, by allowing the removal of dead cells, by promoting otic progenitor differentiation and, interestingly, also neuron axon outgrowth. Our work underlines the relevance of autophagy during early embryonic development as a cell makeover.

Materials and Methods

Chicken embryos. Chicken embryos were obtained from fertilized eggs from a local farm (Granja Santa Isabel, Cordoba, Spain) and were incubated in a humidified atmosphere at 37.8 °C. Embryos were staged as HH17, HH18 and HH19 according to Hamburger and Hamilton's (HH) criteria.[41]

Isolation, organotypic culture and treatment of OVs and AVG. Early inner ear *ex vivo* development can be followed by dissection of otocysts from the embryo and incubation in a defined culture medium to study the molecules and processes that instruct the cellular diversity found *in vivo*.[42] Embryos at stage HH18 (65 h of incubation) were obtained and the OVs were dissected from the surrounding tissue with sharpened tungsten needles. They were transferred into four-well culture plates (Nunc, Roskilde, Denmark) and then incubated at 37 °C in a water-saturated atmosphere containing 5% CO_2. The standard culture medium consisted of M199 medium with Earle's salts (Sigma-Aldrich, Saint Louis, MO, USA) supplemented with 2 mM glutamine (Gibco, Paisley, UK) and antibiotics (50 IU/ml penicillin (Ern, Barcelona, Spain) and 50 μg/ml streptomycin (CEPA, Madrid, Spain)). AVG were obtained from stage HH19$^+$ chicken embryos (82 h of incubation) dissected out aseptically and plated onto glass cover slips that had been previously coated with poly-D-lysine and fibronectin.[43] The AVG was cultured in 0.25 ml F12/Dulbecco's modified Eagle medium (Gibco) containing 100 μg/ml transferrin, 16 μg/ml putrescine, 6 ng/ml progesterone, 5.2 ng/ml sodium selenite (all from Sigma) and antibiotics as above. *Ex vivo* cultures were performed as previously reported by us and others to study inner ear development in several species, including the chicken.[44–47] Explants were treated with IGF-I (10 nM, recombinant IGF-I, Roche Molecular Biochemicals, Basel, Switzerland), 3-MA (1 and 10 mM, Sigma-Aldrich), MP (10 mM, Sigma-Aldrich), CQ (10 μM; Sigma-Aldrich), or a pan-caspase inhibitor Boc-D-FMK (BOC; 50 and 100 μM, Calbiochem, La Jolla, CA) for the times indicated in the Results section by following procedures previously published.[5,7,48] The solvent used (DMSO) had no detectable effects on cultured OVs. OVs cultured in serum-free medium without additives were used as controls (0S). To knockdown gene expression, antisense morpholino oligonucleotides (MO) were used. LC3B and standard control FITC-conjugated morpholinos were obtained from Gene Tools, LLC (Philomath, OR, USA). HH18 OV cultures were incubated as recommended by the manufacturer with Endo-Porter solution (0.4%) to facilitate MO's delivery and with either 20 μM of the FITC-conjugated or LC3B-specific (GCTTGAAGCTCTTCTCCGAGGGCAT) MO for 20 h. For immunostaining and Tdt-mediated dUTP nick-end labeling (TUNEL) labeling, OVs were fixed for 2 h in 4% (w/v) paraformaldehyde (Merck Chemicals, Mollet del Valles, Spain) at 4 °C.

AVG and OV areas were measured using the ImageJ software (Wayne Rasband, National Institutes of Health, Bethesda, MD, USA). The data are shown as a ratio of the values of AVG area related to the total explant (OV + AVG) area and were normalized to the 0S condition, which was given an arbitrary value of 100. The data are presented as the mean ± S.E.M. and the statistical significance was estimated with the Student's *t*-test.

Quantitative RT-PCR. OVs from chicken embryos were pooled to obtain RNA at different developmental stages: HH17 ($n = 40$), HH18 ($n = 25$) and HH19 ($n = 20$). Three independent RNA pools from each stage were isolated with TRIZOL (Invitrogen, Carlsbad, CA, USA) following the manufacturer's instructions, and the integrity and concentration of the RNA was assessed with an Agilent Bioanalyzer 2100 (Agilent Technologies, Santa Clara, CA, USA). cDNA was then generated by reverse transcription (High Capacity cDNA Reverse Transcription Kit; Applied Biosystems, Foster City, CA, USA). Real-time PCR of each pool was performed in triplicate using specific oligonucletides from 'Quantitec Primer Assays' for chicken *Atg5* and *Beclin-1* (Gg_ATG5_1_SG (QT00647038), Gg_BECN1_1_SG (QT00634753); Geneglobe, Qiagen, Hilden, Germany) and using SYBR Green as the detection system. PCR was performed on an Applied Biosystems 7900HT Real-Time PCR System using eukaryotic 18S rRNA as the endogenous housekeeping gene (Hs99999901_s1, TaqMan, Applied Biosystems). The estimated gene expression was calculated as $2^{-\Delta\Delta Ct}$ and statistical significance was estimated using the Student's *t*-test.

Western blotting. OVs (HH18) were isolated and cultured at 37 °C in serum-free M199 culture medium or with the inhibitors 3-MA (10 mM) for 20 h or CQ (10 μM) for the last 4 h of culture. Forty OVs from each condition were homogenized in ice-cold Laemmli buffer with 50 mM dithiotreitol, Phosphatase Inhibitor Cocktail 2 and Protease Inhibitor Cocktail (both 1 : 100, from Sigma-Aldrich). The homogenized samples were heated at 95 °C for 5 min and frozen immediately. Gels were loaded with solutions containing equal amounts of proteins and the OV protein extracts were resolved by SDS-PAGE on 12% polyacrylamide gels. The proteins were transferred to nitrocellulose membranes and after incubation with blocking solution (5% non-fat dry milk in TRIS-buffered saline with 0.1% Tween-20: TBS-T), the membranes were probed overnight at 4 °C with the appropriate specific primary antibodies (Supplementary Table S1). The membranes were subsequently washed and then incubated with the appropriate peroxidase-conjugated secondary antibody (1 : 3000) for 1 h at RT. Western blot films were scanned and the bands were quantified by densitometry with Image J software. At least three independent experiments were performed per condition.

Immunohistofluorescence. The sources, dilution and cell specificities of the antibodies used for immunofluorescent staining are shown in Supplementary Table S1. Samples were washed and permeabilized in 1% PBS/Triton-X-100 (PBS-T), and they were exposed to the primary antibodies overnight at 4 °C. Non-specific binding sites were blocked for 1 h in PBS-T, 3% (wt/vol) BSA (Sigma-Aldrich) and 5% (vol/vol) normal goat serum.

LysoTracker Red (LTR; Invitrogen) staining was performed during the last 15 min of OV culture by adding 1 μM at 37 °C. OVs were washed, permeabilized and stained with TUNEL as described below. Annexin-V staining (Chemicon, Pittsburg, MA, USA) was performed following the manufacturer's instructions. Briefly, annexin-V-biotin was added to the cultures for the last 30 min of organotypic culture. OVs were then washed, fixed for 2 h in 4% (w/v) paraformaldehyde (Merck) at 4 °C and stained for TUNEL as described below. After the TUNEL reaction, the OVs were further incubated with the secondary antibody.

The secondary antibodies were incubated for 2 h at room temperature. For dual-fluorescence immunolabeling, OVs were incubated with Alexa Fluor 488 goat anti-mouse (1 : 200), Alexa Fluor 647 goat anti-rabbit and/or Alexa Fluor 546 goat anti-rabbit secondary antibodies (1 : 200; all from Molecular Probes, Eugene, OR, USA). For whole-mount immunofluorescence, OVs were incubated with the secondary antibodies for 3 h at room temperature. Sections and whole-OVs were mounted in Prolong Gold with DAPI (4′,6-diamidino-2-phenylindole; Invitrogen) and visualized by fluorescence (Nikon 90i, Tokyo, Japan) or confocal microscopy (Leica TCS SP2, Wetzlar, Germany). At least 5–6 OV explants or frozen sections were analyzed for each condition obtained in at least two independent experiments.

BrdU incorporation and immunodetection. To study cell proliferation, OVs were incubated with 5-bromo-2′-deoxyuridine (BrdU; Sigma-Aldrich), a thymidine analog that is incorporated into DNA during the S phase of the cell cycle. BrdU (10 mg/ml) was added to the culture medium at different times as indicated (45 min, 1, 3 or 6 h) before the end of the incubation and its incorporation was detected with a specific antibody as above, but including a DNA denaturation step as recommended by the manufacturer (incubation in 50% (v/v) formamide-SSC, 40 min at 65 °C and in HCl 2 N, 30 min at 37 °C, with a wash for 10 min in pH 8 Tris 0.1 M). At least 5–6 OVs were assayed per condition in two independent experiments.

Monodansylcadaverine staining. Monodansylcadaverine (MDC; 100 μM, Fluka) was added to the medium during the last hour of culture. OVs were then fixed for 2 h in 4% (w/v) paraformaldehyde (Merck) and mounted in Vectashield (Vector, Peterborough, UK). Visualization was carried out by confocal microscopy (Leica TCS SP2). At least 5–6 OVs were analyzed for each condition from at least three independent experiments.

Analysis of programmed cell death. The pattern of cell death in the OV was studied by TUNEL of fragmented DNA using the kit Dead-End Fluorometric TUNEL System (Promega, Madison, WI, USA) essentially as described by the manufacturer and adapted to whole-organ labeling.[29] OVs were mounted with Prolong Gold with DAPI (Invitrogen) and visualized on a confocal microscope (Leica, TCS SP2). TUNEL-positive cells were counted using Image Analysis Software (Olympus, Tokyo, Japan) attributing a value of 100 to the 0S condition. At least five OVs were assayed per condition in three independents experiments. The data are presented as the mean ± S.E.M. and the statistical significance was estimated with the Student's *t*-test.

Electron microscopy. OVs were dissected, fixed in 2% glutaraldehyde in phosphate buffer, postfixed in osmium tetroxide and embedded in araldite. For light microscopy, semithin sections were obtained and stained with toluidine blue. For transmission electron microscopy, ultrathin sections were stained with lead citrate and examined with a Philips EM208 electron microscope (Philips, Eindhoven, The Netherlands).

Conflict of Interest

The authors declare no conflict of interest.

1. Rubel EW, Fritzsch B. Auditory system development: primary auditory neurons and their targets. *Annu Rev Neurosci* 2002; **25**: 51–101.

2. Magariños M, Contreras-Rodríguez J, Aburto MR, Varela-Nieto I. Early development of the vertebrate inner ear. *Anat Rec* 2012 (in press).

3. Fekete DM, Wu DK. Revisiting cell fate specification in the inner ear. *Curr Opin Neurobiol* 2002; **12**: 35–42.

4. Kelley MW. Regulation of cell fate in the sensory epithelia of the inner ear. *Nat Rev Neurosci* 2006; **7**: 837–849.

5. Camarero G, Leon Y, Gorospe I, De Pablo F, Alsina B, Giraldez F et al. Insulin-like growth factor 1 is required for survival of transit-amplifying neuroblasts and differentiation of otic neurons. *Dev Biol* 2003; **262**: 242–253.

6. Sanchez-Calderon H, Rodriguez-de la Rosa L, Milo M, Pichel JG, Holley M, Varela-Nieto I. RNA microarray analysis in prenatal mouse cochlea reveals novel IGF-I target genes: implication of MEF2 and FOXM1 transcription factors. *PLoS ONE* 2010; **5**: e8699.

7. Aburto MR, Magariños M, Leon Y, Varela-Nieto I, Sanchez-Calderon H. AKT signaling mediates IGF-I survival actions on otic neural progenitors. *PLoS ONE* 2012; **7**: e30790.

8. Murillo-Cuesta S, Camarero G, González-Rodríguez A, De La Rosa LR, Burks DJ, Avendaño C et al. Insulin receptor substrate 2 (IRS2)-deficient mice show sensorineural hearing loss that is delayed by concomitant protein tyrosine phosphatase 1B (PTP1B) loss of function. *Mol Med* 2012; **18**: 260–269.

9. Murillo-Cuesta S, Rodríguez-de la Rosa L, Cediel R, Lassaletta L, Varela-Nieto I. The role of insulin-like growth factor-I in the physiopathology of hearing. *Front Mol Neurosci* 2011; **4**: 11.

10. Qu X, Zou Z, Sun Q, Luby-Phelps K, Cheng P, Hogan RN et al. Autophagy gene-dependent clearance of apoptotic cells during embryonic development. *Cell* 2007; **128**: 931–946.

11. Mellén MA, de la Rosa EJ, Boya P. The autophagic machinery is necessary for removal of cell corpses from the developing retinal neuroepithelium. *Cell Death Differ* 2008; **15**: 1279–1290.

12. Ravikumar B, Sarkar S, Davies JE, Futter M, Garcia-Arencibia M, Green-Thompson ZW et al. Regulation of mammalian autophagy in physiology and pathophysiology. *Physiol Rev* 2010; **90**: 1383–1435.

13. Mizushima N, Levine B. Autophagy in mammalian development and differentiation. *Nat Cell Biol* 2010; **12**: 823–830.

14. Montero JA, Hurlé JM. Sculpturing digit shape by cell death. *Apoptosis* 2010; **15**: 365–375.

15. Aburto MR, Hurlé JM, Varela-Nieto I, Magariños M. Autophagy during vertebrate development. *Cells* 2012; **1**: 428–448.

16. Chen N, Karantza V. Autophagy as a therapeutic target in cancer. *Cancer Biol Ther* 2011; **11**: 157–168.

17. Wong E, Cuervo AM. Autophagy gone awry in neurodegenerative diseases. *Nat Neurosci* 2010; **13**: 805–811.

18. Yang Z, Klionsky DJ. Eaten alive: a history of macroautophagy. *Nat Cell Biol* 2010; **12**: 814–822.

19. Ferraro E, Cecconi F. Autophagic and apoptotic response to stress signals in mammalian cells. *Arch Biochem Biophys* 2007; **462**: 210–219.

20. Kuma A, Hatano M, Matsui M, Yamamoto A, Nakaya H, Yoshimori T et al. The role of autophagy during the early neonatal starvation period. *Nature* 2004; **432**: 1032–1036.

21. Komatsu M, Waguri S, Ueno T, Iwata J, Murata S, Tanida I et al. Impairment of starvation-induced and constitutive autophagy in Atg7-deficient mice. *J Cell Biol* 2005; **169**: 425–434.

22. Yue Z, Jin S, Yang C, Levine AJ, Heintz N. Beclin 1, an autophagy gene essential for early embryonic development, is a haploinsufficient tumor suppressor. *Proc Natl Acad Sci USA* 2003; **100**: 15077–15082.

23. Fimia GM, Stoykova A, Romagnoli A, Giunta L, Di Bartolomeo S, Nardacci R et al. Ambra1 regulates autophagy and development of the nervous system. *Nature* 2007; **447**: 1121–1125.

24. Rubinsztein DC, Gestwicki JE, Murphy LO, Klionsky DJ. Potential therapeutic applications of autophagy. *Nat Rev Drug Discov* 2007; **6**: 304–312.

25. Mariño G, Fernández AF, Cabrera S, Lundberg YW, Cabanillas R, Rodríguez F et al. Autophagy is essential for mouse sense of balance. *J Clin Invest* 2010; **120**: 2331–2344.

26. Taylor RR, Nevill G, Forge A. Rapid hair cell loss: a mouse model for cochlear lesions. *J Assoc Res Otolaryngol* 2008; **9**: 44–64.

27. Klionsky DJ, Abeliovich H, Agostinis P, Agrawal DK, Aliev G, Askew DS et al. Guidelines for the use and interpretation of assays for monitoring autophagy in higher eukaryotes. *Autophagy* 2008; **4**: 151–175.

28. Schutters K, Reutelingsperger C. Phosphatidylserine targeting for diagnosis and treatment of human diseases. *Apoptosis* 2010; **15**: 1072–1082.

29. Magariños M, Aburto MR, Sánchez-Calderón H, Muñoz-Agudo C, Rapp UR, Varela-Nieto I. RAF kinase activity regulates neuroepithelial cell proliferation and neuronal progenitor cell differentiation during early inner ear development. *PLoS One* 2010; **5**: e14435.

30. Puligilla C, Dabdoub A, Brenowitz SD, Kelley MW. Sox2 induces neuronal formation in the developing mammalian cochlea. *J Neurosci* 2010; **30**: 714–722.

31. Li H, Liu H, Sage C, Huang M, Chen ZY, Heller S. Islet-1 expression in the developing chicken inner ear. *J Comp Neurol* 2004; **477**: 1–10.

32. Sanchez-Calderon H, Milo M, Leon Y, Varela-Nieto I. A network of growth and transcription factors controls neuronal differentiation and survival in the developing ear. *Int J Dev Biol* 2007; **51**: 557–570.

33. Lum JJ, DeBerardinis RJ, Thompson CB. Autophagy in metazoans: cell survival in the land of plenty. *Nat Rev Mol Cell Biol* 2005; **6**: 439–448.

34. Mariño G, Madeo F, Kroemer G. Autophagy for tissue homeostasis and neuroprotection. *Curr Opin Cell Biol* 2011; **23**: 198–206.

35. Maiuri MC, Zalckvar E, Kimchi A, Kroemer G. Self-eating and self-killing: crosstalk between autophagy and apoptosis. *Nat Rev Mol Cell Biol* 2007; **8**: 741–752.

36. Martín-Partido G, Navascués J. Macrophage-like cells in the presumptive optic pathways in the floor of the diencephalon of the chick embryo. *J Neurocytol* 1990; **19**: 820–832.

37. Cecconi F, Levine B. The role of autophagy in mammalian development: cell makeover rather than cell death. *Dev Cell* 2008; **15**: 344–357.

38. Zeng M, Zhou J-N. Roles of autophagy and mTOR signaling in neuronal differentiation of mouse neuroblastoma cells. *Cell Signal* 2008; **20**: 659–665.

39. Ogura K-I, Goshima Y. The autophagy-related kinase UNC-51 and its binding partner UNC-14 regulate the subcellular localization of the Netrin receptor UNC-5 in *Caenorhabditis elegans*. *Development* 2006; **133**: 3441–3450.

40. Rodríguez-Muela N, Germain F, Mariño G, Fitze PS, Boya P. Autophagy promotes survival of retinal ganglion cells after optic nerve axotomy in mice. *Cell Death Differ* 2011; **19**: 162–169.

41. Hamburger V, Hamilton HL. A series of normal stages in the development of the chick embryo. 1951. *Dev Dyn* 1992; **195**: 231–272.

42. Davies D. Temporal and spatial regulation of alpha6 integrin expression during the development of the cochlear-vestibular ganglion. *J Comp Neurol* 2007; **502**: 673–682.

43. Davies D. Cell-extracellular matrix versus cell-cell interactions during the development of the cochlear-vestibular ganglion. *J Neurosci Res* 2011; **89**: 1375–1387.

44. León Y, Vazquez E, Sanz C, Vega JA, Mato JM, Giraldez F et al. Insulin-like growth factor-I regulates cell proliferation in the developing inner ear, activating glycosyl-phosphatidylinositol hydrolysis and Fos expression. *Endocrinology* 1995; **136**: 3494–3503.

45. Garrido JJ, Schimmang T, Represa J, Giraldez F. Organoculture of otic vesicle and ganglion. *Curr Top Dev Biol* 1998; **36**: 115–131.

46. Miura T, Shiota K, Morriss-Kay G. A mesenchyme-free culture system to elucidate the mechanism of otic vesicle morphogenesis. *J Anat* 2004; **205**: 297–312.

47. Fantetti KN, Fekete DM. Dissection and culture of chick statoacoustic ganglion and spinal cord explants in collagen gels for neurite outgrowth assays. *J Vis Exp* 2011; doi:10.3791/3600.

48. Frago LM, Cañón S, de la Rosa EJ, León Y, Varela-Nieto I. Programmed cell death in the developing inner ear is balanced by nerve growth factor and insulin-like growth factor I. *J Cell Sci* 2003; **116**: 475–486.

Supplementary Information accompanies the paper on Cell Death and Disease website (http://www.nature.com/cddis)